

A Coupled Vegetation–Soil Bidirectional Reflectance Model for a Semiarid Landscape

Wenge Ni* and Xiaowen Li†

A model for the bidirectional reflectance over soils is coupled with a vegetation reflectance model to predict the bidirectional reflectance of semiarid landscape. The vegetation model is a hybrid of geometric optical and radiative transfer (GORT) model for bidirectional reflectance over discontinuous plant canopies. The coupling is done by relaxing the assumption of Lambertian background into a non-Lambertian case in the vegetation GORT model. The non-Lambertian soil background is modeled by a soil BRDF model. The coupled model is validated with POLDER and AVHRR imagery collected in a semiarid site during the Jornada PROVE'97 campaign with good accuracy. It is a very simple but analytical model for bidirectional reflectance over a semiarid landscape and has the potential for surface parameter retrieval for the study of biosphere–atmosphere interaction. ©Elsevier Science Inc., 2000

INTRODUCTION

Savannas, shrublands, and woodlands cover more than one-fourth of the global vegetated land surface (Asner et al., 1997). Usually those areas consist of varied mixtures of herbaceous vegetation and scattered woody shrubs or trees. Recently, those regions have experienced degradation, that is, the changing of grasses to shrubs due to persistent drought, overgrazing, and fire suppression (Schlesinger et al., 1990).

Shrublands and herbaceous vegetation contribute differently to biogeochemical processes and the energy transfer between the landsurface and the atmosphere. The shift

from grasslands to shrublands will affect the biogeochemical cycles and the interactions between the land surface and the atmosphere over those regions. Satellite remote sensing provides the only technically consistent and temporally regular means of monitoring those changes at regional scales and estimating landsurface biophysical parameters (Sellers et al., 1994).

The land surface scatters solar radiation anisotropically. Even for the same location, for different overpasses, satellites receive reflected solar radiation signals differently due to changing viewing or illumination angles. This anisotropic effect is described in Eq. (1) by the bidirectional reflectance distribution function (BRDF), which is defined as the ratio of the radiance scattered by a surface into a given direction to the incident irradiance (radiant power per unit area of surface) (Nicodemus et al., 1977):

$$BRDF(\theta_i, \varphi_i; \theta_v, \varphi_v) \equiv \frac{dL_r(\theta_v, \varphi_v)}{L_i(\theta_i, \varphi_i) d\Omega_i} = \frac{dL_r(\theta_v, \varphi_v)}{dE_i(\theta_i, \varphi_i)}, \quad (1)$$

where θ_i and φ_i are the solar zenith and azimuth angles, θ_v and φ_v are the viewing zenith and azimuth angles, the projected solid angle $\Omega \equiv \int_{\omega} \cos \theta d\omega = \int_{\omega} \cos \theta \sin \theta d\theta d\varphi$, is in the unit of sr, L is the radiance, and E is the irradiance. BRDF is in the unit of $(\text{sr})^{-1}$.

In reality, bidirectional reflectance factor (BRF) is the most closest possible field measurement to the fundamental BRDF. BRF is defined as the ratio of the reflectance of the surface to that of a perfectly Lambert surface under the same conditions of illumination and viewing directions. The relationship between BRDF and BRF is $BRF(\theta_i, \varphi_i; \theta_v, \varphi_v) \equiv \pi BRDF(\theta_i, \varphi_i; \theta_v, \varphi_v)$. BRF is dimensionless. In this study, we refer to BRF as bidirectional reflectance, $R(\theta_i, \theta_v, \varphi)$, where φ is the relative azimuth angle. The importance of the BRDF in remote sensing of the surface of the earth from satellites has been recognized clearly by the remote sensing community (Strahler, 1997).

The interaction of light with plant canopies and background usually involves two physical processes: surface

* Raytheon ITSS and Department of Geography, University of Maryland, 2191 LeFrak Hall, College Park, MD 20742

† Department of Geography and Center for Remote Sensing, Boston University, Boston, Massachusetts

Address correspondence to Wenge Ni, Department of Geography, University of Maryland, 2191 LeFrak Hall, College Park, MD 20742

Received 10 March 1999; revised 28 June 1999.

scattering, which can lead to a hotspot effect, and volume scattering. The primary cause of the hotspot in most vegetation canopies is the absence of shadows observable from the direction of illumination, leading to a brighter scene when viewed from the direction of the sun. This effect is best handled by the theory of geometric optics (GO) (Li and Strahler, 1986; 1992; Strahler and Jupp, 1990). The volume scattering is the multiple scattering within plant canopies, which is best handled by radiative transfer (RT) theory.

The GO models have been applied for discontinuous plant canopies. Any natural vegetation such as forests, shrublands, and woodlands can be considered as discontinuous plant canopies. The clumping, such as clumping of leaves into crowns, in the discontinuous plant canopies results in randomly distributed clumping objects in certain shape in space. The clumping objects cast shadows on each other and the background, which strongly conditions the brightness of the vegetation cover as seen from a given viewpoint in the hemisphere. The shadowing effect was well modeled as a function of the density, size, and shape of the clumping objects using geometric optics. In geometric optical (GO) models, the scene is treated as an assemblage of three-dimensional tree crowns with specific shape and size. The scene as viewed by a sensor has four components: sunlit crown, shaded crown, sunlit background, and shaded background. The bidirectional reflectance is modeled as a linear combination of the spectral signatures of four components, weighted by their areal proportions. The areal proportions are modeled as functions of the shape and size of the clumping objects, their count densities, and illumination and viewing directions (Li and Strahler, 1986; 1992; Strahler and Jupp, 1990).

One question associated with using GO models concerns the estimation of the component spectral signatures. The component spectral signatures are the result of multiple scattering based on radiative transfer. A recently developed hybrid geometric optical and radiative transfer (GORT) model is well suited for the bidirectional reflectance over discontinuous plant canopies (Li et al., 1995). The GORT model combines the geometric optics of large scale canopy structure with principles of radiative transfer for volume scattering within individual crowns. More recently, an analytical GORT model for bidirectional reflectance over discontinuous plant canopies was developed by Ni et al. (1999). It uses the basic structure of the geometric optical model, but analytical approximations of radiative transfer are used to model the reflectance of the components. By this way, the nature of the simplicity of the GO model is retained. It has great potential for inversion (Abuelgasim et al., 1999).

When applying the GORT model in very sparse arid and semiarid landscapes, one question of concern is the effect of bidirectional reflectance from the background. In the original GORT and GO models, the background

is assumed to be Lambertian. However, directional measurements of soil surfaces have indicated that the Lambertian assumption is invalid (Irons et al., 1989). For very sparse arid and semiarid ecosystems, the background contributes to the satellite signal significantly. Ignoring the BRDF effect from the background will lead to inaccurate modeling of the BRDF over the regions. For example, a study for estimation of BRDF over a semiarid ecosystem from AVHRR satellite data was conducted by O'Brien et al. (1998). Two BRDF models were used. One is Staylor and Suttles (1986) model for the bidirectional reflectance over a desert site. It is essentially an empirical model involving four parameters. The model satisfies reciprocity and is flexible. The other one is the semiempirical pure GO model for sparse canopies from the Algorithm for MODIS Bidirectional Reflectance Anisotropy of the Land Surface (AMBRALS) (Wanner et al., 1995), which accounts for the shadowing of tree crowns with the assumption of a Lambertian background. For semiarid targets, the GO model seems more appropriate. Both models show the dependence of reflected radiance on structural properties of the vegetation canopy and soil. But their analysis results show that the pure GO model gave unacceptable fits for semi-arid Australian sites. This is partly due to the semiempirical GO model not taking account for the effect of the soil BRDF. Without accounting for the correct physics, the fitting will be worse for the semiempirical model than the empirical model.

This study explores how the anisotropic effect of soil background contributes to the surface bidirectional reflectance and how it does affect the overall reflectance, that is, the physical principles causing the scattering dynamics in sparse vegetation canopies. In order to do so, a coupled soil-vegetation model for the bidirectional reflectance over a very sparsely vegetated landscape is developed. The analytical GORT model for the bidirectional reflectance over discontinuous plant canopies (Ni et al., 1999) and two soil BRDF models are used. The coupling is accomplished by relaxing the assumption of the Lambertian background in the GORT model to the non-Lambertian case. This coupled model is validated using Advanced Very High Resolution Radiometer (AVHRR) and Polarization and Directionality of the Earth's Reflectances (POLDER) data collected during the Jornada Prototype Validation Exercise (PROVE) campaign in 1997.

In the mixture of varying amounts of woody shrubs and herbaceous plants in the Jornada site, the signatures of the canopy shaded and sunlit components are a mixture of different species (two major species are mesquite and yucca in the transitional site used in the study). In this study, the signatures of the sunlit and shaded crowns are calculated by using integrated values of leaf transmittance and reflectance of the two species weighted by their areal proportion as inputs for the calculation of the signatures of the canopy components. Another way to

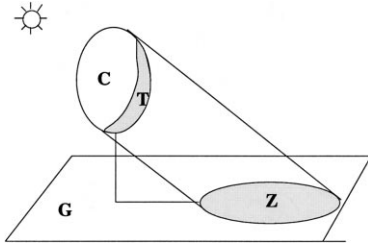


Figure 1. The four scene components used in the geometric optical model: C is sunlit tree crown, T is shaded tree crown, G is sunlit background, and Z is shaded background.

model the signatures of sunlit crown and shaded crowns is using the integrated values of the signatures of sunlit and shaded crown component of each species, which can be calculated based on the values of leaf transmittance and reflectance of each species.

COUPLING OF THE SOIL AND VEGETATION BRDF MODELS

Vegetation Model

Radiation interactions with a plant canopy are affected by many factors, including the source distribution (proportions of incident beam irradiance and diffuse skylight, and its spectral properties) and the canopy structure, as well as the spectral properties of the canopy elements and the canopy background and illumination and viewing geometry. The proportions of beam irradiance and diffuse skylight and its spectral properties depend on atmospheric conditions and wavelength.

In the GORT model, the discontinuous canopy is treated as an assemblage of random distributed clumping objects with ellipsoid shape, and certain count density. The clumping objects in the Jornada site are shrubs, which are in ellipsoid shape. The canopy structure parameters used in the GORT model are: horizontal and vertical object radii (R and b), the object density, the lower and upper height of object centers (h_1 and h_2), and the foliage area volume density within the objects (L_v). The spectral properties of the canopy element and background are the single scattering albedo of canopy elements and background albedo which are spectrally dependent. Four scene components are modeled: sunlit clumping objects, shaded clumping objects, sunlit background, and shaded background (Fig. 1). The bidirectional reflectance of the scene as a whole is modeled as the sum of radiances or reflectances of individual components as weighted by their areal proportions, that is [Eq. (2)],

$$R(\theta_i, \theta_v, \varphi) = K_c C + K_g G + K_t T + K_s Z, \quad (2)$$

where θ_i and θ_v are solar zenith and viewing zenith

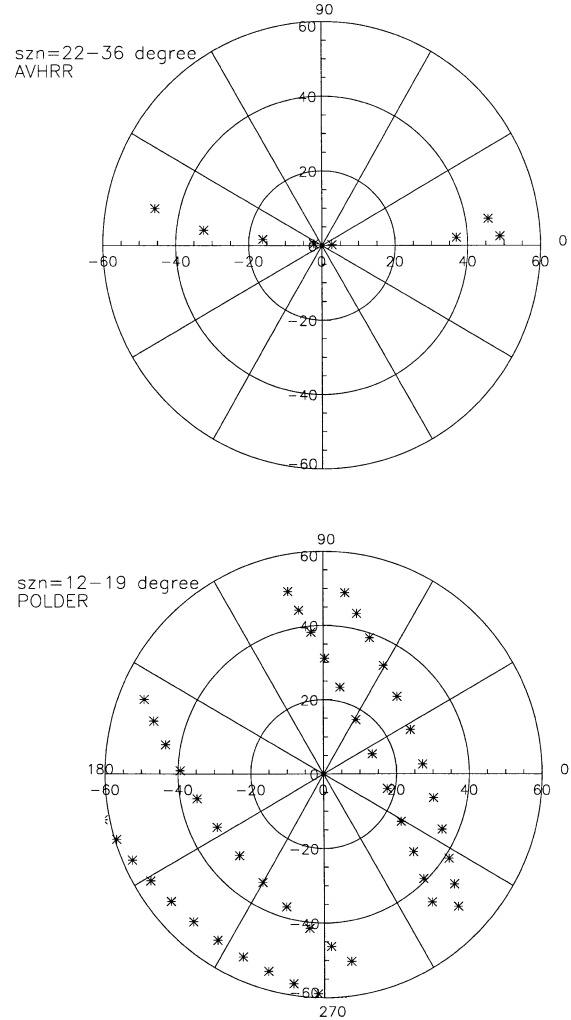


Figure 2. Polar plots of sampling angles of AVHRR and POLDER data collected in the Jornada site. The axes are the viewing azimuth angles, starting from 0° and increasing until 360° in a counterclockwise direction. The distance from the center is the viewing zenith angle at every 20° from 0° (at the center) to 60° .

angles and φ is the relative azimuth angle, K_c is the areal proportion of sunlit and viewed crown, K_g is the areal proportion of the sunlit and viewed background, K_t is the areal proportion of shaded and viewed crown, and K_s is the areal proportion of shaded and viewed background.

Table 1. Canopy Structure Parameters for the GORT Model

	$R(m)$	$b(m)$	$\lambda(1/m^2)$	$h_1(m)$	$h_2(m)$	FAVD
	0.62	0.64	0.1656	0.1	1.18	1.372
R	Horizontal radius of the clumping objects					
b	Vertical radius of the clumping objects					
λ	Count density of the clumping objects					
h_1	Lower bound of the clumping object centers					
h_2	Upper bound of the clumping object centers					
L_v	Foliage area volume density within the clumping object					

Table 2. Spectral Properties of Canopy and Soil Background

	Leaf Reflectance	Leaf Transmittance	Nadir Reflectance of Background
AVHRR ch1 (0.635 μm)	0.090	0.032	0.2470
AVHRR ch2 (0.85 μm)	0.346	0.320	0.3276
Polder ch1 (0.443 μm)	0.073	0.021	0.0996
Polder ch4 (0.670 μm)	0.063	0.021	0.2662
Polder ch5 (0.765 μm)	0.340	0.320	0.3284
Polder ch6 (0.865 μm)	0.346	0.320	0.3353

The quantities K_c , K_g , K_s , and K_t are well modeled as functions of tree geometry and sun and viewing geometry based on the principles of geometric optics as described by Li and Strahler (1992).

The spectral signatures C , G , T , and Z are defined as the brightness of the sunlit crown, sunlit background, shaded crown, and shaded background. They are functions of the proportion of incoming direction beam and diffuse skylight [Eqs. (3), (4), (5), and (6)]:

$$C = f_d C_d + (1 - f_d) C_f, \quad (3)$$

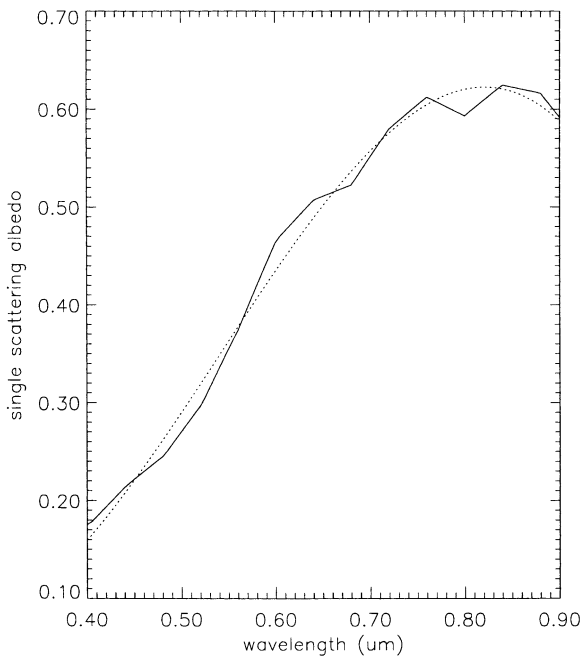
$$T = f_d T_d + (1 - f_d) T_f, \quad (4)$$

$$G = f_d G_d + (1 - f_d) G_f, \quad (5)$$

$$Z = f_d Z_d + (1 - f_d) Z_f, \quad (6)$$

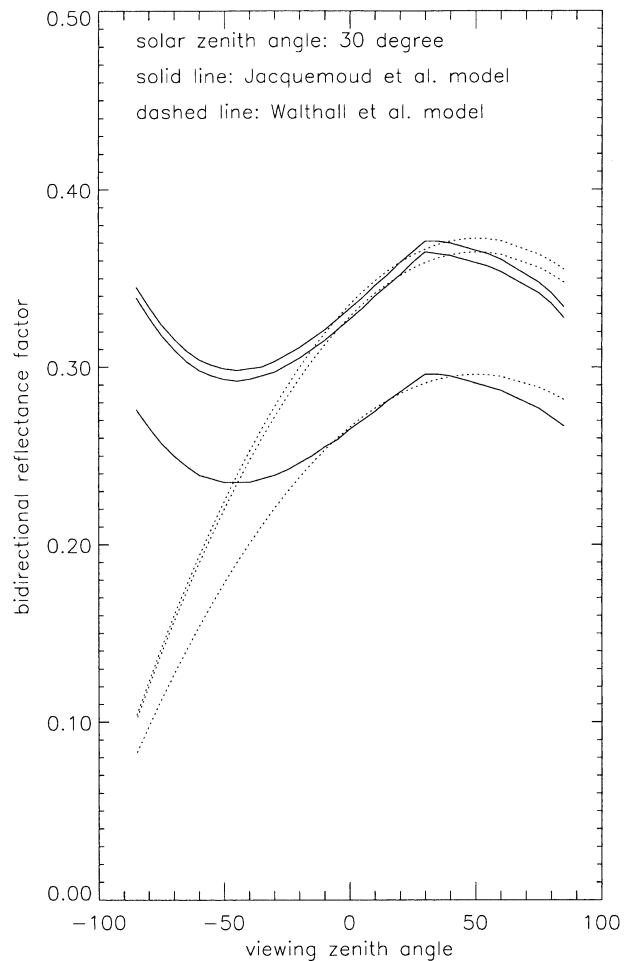
where f_d is the proportion of incident direct beam and the quantities C_d , T_d and Z_d are the contributions by the direct beam, and C_f , T_f , and Z_f are the contributions by the diffuse skylight to the component signatures.

Figure 3. Single scattering albedo of soil scattering elements in the Jornada site (solid line) and its polynomial fit (dash line). They are the inputs for the Jacquemoud et al. (1992) soil BRDF model.



- G_d and G_f were simply modeled by background albedo since the background is simply assumed to be Lambertian in the original version. In this study, the assumption of Lambertian background is relaxed. The BRDF values predicted from soil models are used for G_d (see the following section on the soil model).
- Z_d and Z_f are modeled by the light scattered and

Figure 4. Comparison of the bidirectional reflectance factor modeled by Jacquemoud and Walthall soil bidirectional reflectance models at different wavelengths. The lines from top to bottom are for wavelengths 0.87 μm , 0.765 μm , and 0.67 μm .



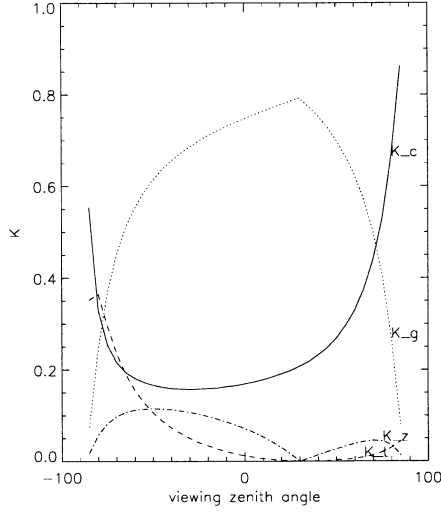


Figure 5. Areal proportion of four components in GO models including the sunlit background (K_g), the sunlit crown (K_c), the shaded background (K_s), and the shaded crown (K_z). The solar zenith angle is 30° . Positive viewing zenith angles indicate backward scattering and negative values for forward scattering.

directly passing through the within-crown gaps and reflected by the background.

- C_d and C_f are composed of three components [Eqs. (7) and (8)]:

$$C_d = C_d^c + C_d^f + C_d^{c \leftrightarrow f}, \quad (7)$$

$$C_f = C_f^c + C_f^f + C_f^{c \leftrightarrow f}, \quad (8)$$

C_d^c and C_f^c are modeled by the path reflectance within the canopy layer and the hotspot function at finer canopy level, such as branch, stem and leaf levels. C_d^f and C_f^f are the first-order scattered radiance from the background. $C_d^{c \leftrightarrow f}$ and $C_f^{c \leftrightarrow f}$ are the multiple scattering between the canopy layer and the background.

- T_d and T_f are modeled by the light scattered back and forth between the background and the canopy layer.

By tracking the multiple scattering within crowns and the scattering between canopy layer and background, the component signatures are modeled as functions of the analytical approximation of radiative transfer within a plant canopy and the background reflectance. The finer level hotspot, such as the hotspot by leaf, branch, and trunk levels, is included in the spectral signature of sunlit crown through bidirectional within-crown gap probability. Using this approach, the model captures the multilevel hotspot effect for discontinuous plant canopies, and the multiple scattering based on radiative transfer. The geometric optical model captures the

mutual shadowing effect at crown level, and the finer level hotspot function captures the mutual shadowing effect at finer canopy structure level, such as leaf, branch, and trunk levels.

The Soil BRDF Model

The BRDF effect over soil has been widely studied. Analysis in laboratory (Irons et al., 1989) and field measurements have shown the anisotropic effect of soil depending on soil constituents, such as mineral composition, organic matter, iron oxides, and soluble salts. The surface roughness and soil moisture also are important factors. Surface roughness influences shadows and the soil moisture influences the optical properties from the visible to the middle infrared. Many models for the bidirectional reflectance over soil have been developed. In this study, two soil models are used: One is the analytical model originally developed by Hapke (1981) for planetary surface reflectance, and then inverted by Jacquemoud et al. (1992) to retrieve the soil physical parameters. The other is an empirical model originally developed by Walthall et al. (1985), and later modified by Nilson and Kuusk (1989) to satisfy the reciprocity.

The Hapke Model

Hapke (1981) modeled the bidirectional reflectance over soil as in Eqs. (9), (10), and (11):

$$R_s(\theta_i, \theta_v, \varphi) = \frac{\omega}{4} \frac{\mu_i}{\mu_i + \mu_v} \{ [1 + B(g)] P(g, g') + H(\mu_i) H(\mu_v) - 1 \}, \quad (9)$$

where $\mu_i = \cos(\theta_i)$, $\mu_v = \cos(\theta_v)$, ω is the single scattering albedo of the soil elements,

$$H(x) = \frac{1 + 2x}{1 + 2\sqrt{1 - \omega x}}, \quad (10)$$

$$B(g) = \frac{1}{1 + \frac{1}{h} \tan(\frac{g}{2})}. \quad (11)$$

In the original Hapke model, the phase function P is only a function of phase angle, g describing the angular distribution of the light scattered by a terrestrial surface. Jacquemoud et al. (1992) parametrized P as a function of phase angle g and the angle between the specular and the outgoing light directions, g' . By this approach, the phase function explains both the backscattering and forward scattering (the specular effect) by the smooth soil, that is [Eqs. (12), (13), (14), and (15)].

$$P(g, g') = 1 + b \cos(g) + c \frac{3 \cos^2 g - 1}{2} + b' \cos(g') + c' \frac{3 \cos^2 g' - 1}{2} \quad (12)$$

with

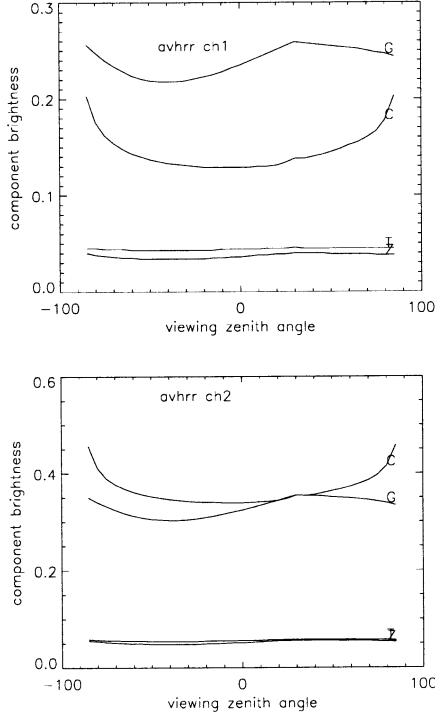


Figure 6. The signatures of four components in GO models at AVHRR Channels 1 and 2 including the sunlit background (G), sunlit crown (C), shaded background (Z), and shaded crown (T).

$$\int_{4\pi} P(g, g') \frac{d\Omega}{4\pi} = 1, \quad (13)$$

$$\cos g = \mu_i \mu_v + \sqrt{1 - \mu_i^2} \sqrt{1 - \mu_v^2} \cos \varphi, \quad (14)$$

$$\cos g' = \mu_i \mu_v - \sqrt{1 - \mu_i^2} \sqrt{1 - \mu_v^2} \cos \varphi. \quad (15)$$

The final formulation of the bidirectional soil reflectance requires the following six parameters: ω , h , b , c , b' , c' , where only ω is a spectral-dependent soil parameter, h is the roughness parameter, and b , c , b' , c' are phase function parameters, which are mainly functions of the refractive indices. The parameters are usually derived from the field measurements of the directional soil reflectance.

The Walthall Model

Walthall et al. (1985) proposed an empirical formula for soil BRDF, which is valid for soils of average roughness. The formula agrees well with soil reflectance measurements. Nilson and Kuusk (1989) modified it to satisfy the reciprocity, in the form of Eq. (16):

$$R_s(\theta_i, \theta_v, \varphi) = \frac{\rho_s(\theta_i, 0, 0)}{e_0(\theta_i)} [e_0(\theta_i) + e_1(\theta_i) \theta_v \cos(\varphi) + e_2(\theta_i) \theta_v^2] \quad (16)$$

where [Eqs. (17), (18), and (19)]

$$e_0(\theta_i) = 16.41 - 4.3 \theta_i^2, \quad (17)$$

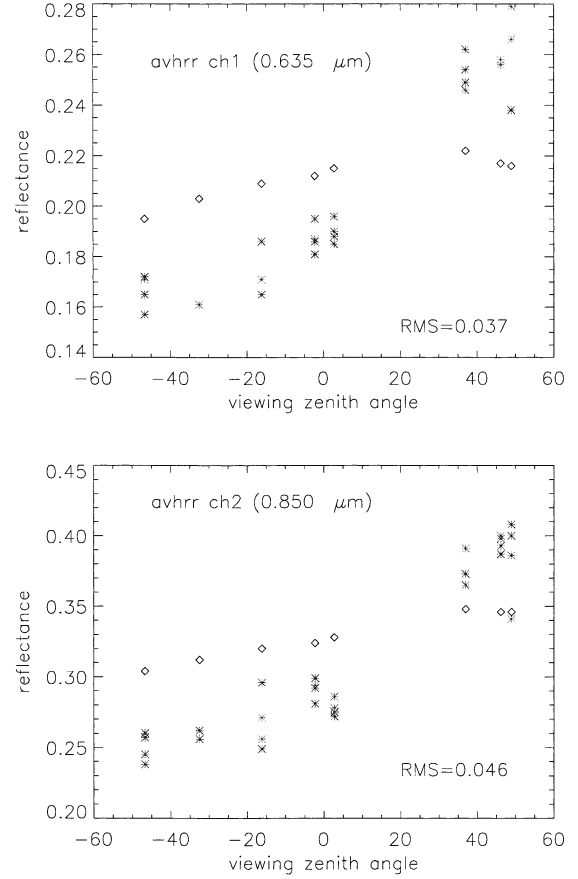


Figure 7. Comparison of the model prediction using the GORT vegetation model with the Lambertian assumption of soil background with AVHRR measurements at the Jornada transition site. The stars are the AVHRR measurements and the diamonds are the model predictions.

$$e_1(\theta_i) = 7.363 \theta_i, \quad (18)$$

$$e_2(\theta_i) = -4.3 + 7.702 \theta_i^2. \quad (19)$$

The only input parameter is the nadir reflectance at the solar zenith angle θ_i , $\rho_s(\theta_i, 0, 0)$.

The Coupled Vegetation–Soil BRDF Model

The Hapke and Walthall soil models are coupled into the GORT vegetation model by relaxing the Lambertian assumption of the soil background in the GORT model to accommodate the non-Lambertian case. The background albedo used in the GORT model is replaced by the bidirectional reflectance of soil calculated from Hapke model or Walthall model.

The coupling of the vegetation and soil BRDF models allows the calculation of the surface bidirectional reflectance over a scene composed of discrete plant canopies. It also allows us to analyze the contribution of the bidirectional reflectance from different scene components.

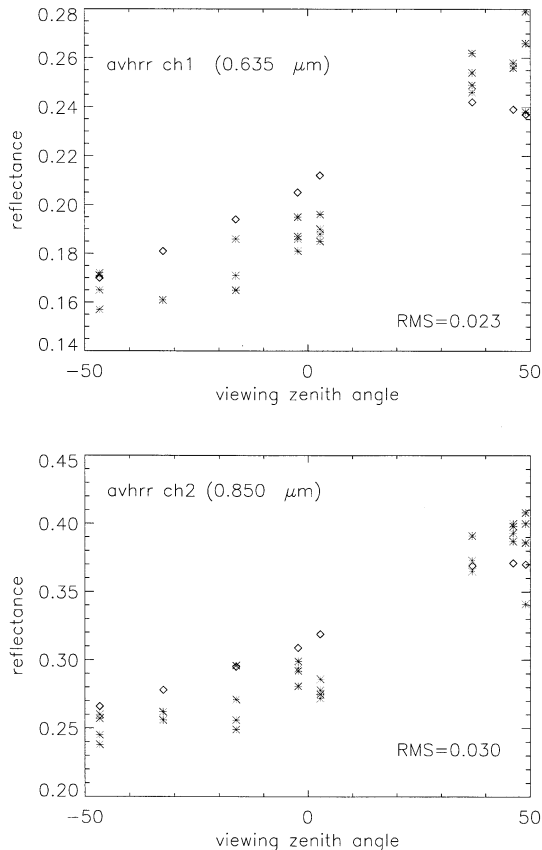


Figure 8. Comparison of the prediction of the surface directional reflectance using a coupled soil-vegetation model with AVHRR measurements at the Jornada transition site in the principal plane. The stars are the AVHRR measurements and the diamonds are the GORT-Hapke model prediction.

MODEL PREDICTIONS AND COMPARISONS WITH FIELD MEASUREMENTS

Study Site

The Prototype Validation Exercise (PROVE) campaign, an activity of the NASA Earth Observing System AM-1 validation program, is one of a series of field research projects designed to thoroughly, yet rapidly and economically, characterize site surface and atmospheric conditions. The goal of PROVE is to provide field context for validation of airborne and satellite data in a consistent fashion over a network of global validation test sites. A PROVE campaign was conducted in desert shrublands in The Jornada Experiment Range (JORNEX) (Privette et al., 1999).

JORNEX is located in a semidesert grassland near Las Cruces, NM (32°30'N, 106°52'W) in the northern Chihuahuan Desert, and ecosystem covering about 26 million acres in the Southwestern United States and Northern Mexico. This is the most arid of the North American grassland regions, with a mean annual precipi-

tation of 25 cm. The study site is in the Southern Jornada Del Muerto Plain in south central New Mexico. The area includes the study site of the Jornada Long-Term Ecological Research (LTER) Project.

During the field campaign of PROVE of 22–30 May 1997, a short but reasonably intensive data collection effort was conducted. Data were collected in three sites: grassland, shrubland, and the transitional site. The validation is conducted using the data collected in the transitional site, which is characterized by an open shrub canopy dominated by mesquite (*Prosopis grandulosa*, 70%), Mormon Tea (*Ephedra aspera*, 20%), and Yucca (*Yucca Glauca*, 10%). Forb and grass species exist in small numbers. The ground measurements of leaf optical properties, soil reflectance, and fractional PAR absorption ($fAPAR$), and leaf area index (LAI) were conducted by Asner et al. (1999) during the field campaign.

Remote sensing satellite data over different spectral, angular and spatial ranges with AVHRR and POLDER were also collected. In this study, the model is validated with both AVHRR and POLDER satellite data. The NOAA-14AVHRR data set are at 1.1 km spatial resolution, with eight observations at varying illumination and viewing directions. The sampling angles for AVHRR sensor during 22–27 May 1997 are almost in the principle plane (see Fig. 2A). Similarly, POLDER observations at 6.5 km spatial resolution include four passes with clear conditions over Jornada obtained during the field campaign. The angular samplings for POLDER sensor are shown in Figure 2B. The atmospheric correction of AVHRR imagery was done by Privette et al. (2000) and the atmospheric correction of POLDER imagery was done by Leroy et al. (personal communication). The aerosol optical thickness required for atmospheric correction were taken from the measurements of a CIMEL sunphotometer mounted at the top of the 100-ft flux tower located at the transitional site (Holben et al., 1998; Privette et al., 2000). The aerosol optical thickness during the field campaign varies from 0.05 to 0.15. This indicates the most incoming solar radiation is direct beam.

The spatial variability study using variogram and wavelet in Jornada site by Pelgrum et al. (1998) showed that the largest scale in all wavelength at the transition site is less than 100 m. When the satellite scales are larger than the length scale of the study site, the scaling effects on the BRDF are the same. Since both 1.1 km spatial resolution of the AVHRR sensor and 6.5 km spatial resolution of the POLDER sensor are much larger than the length scale of the transition site, the scaling effects due to different space sampling are the same. There is not much differences on BRDFs measured from both scales. The study on the spatial variability of surface albedo in the Jornada site by Barnsley et al. (2000) confirm this. Their studies show very close albedo values derived from AVHRR and POLDER data in Jor-

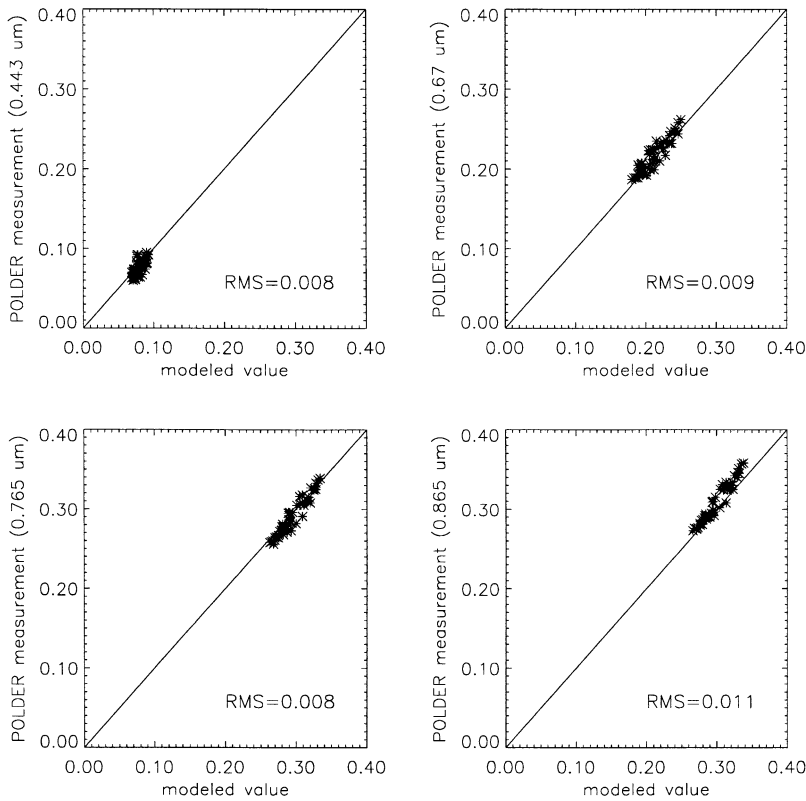


Figure 9. Comparison of the prediction of the surface directional reflectance using a coupled soil-vegetation model with POLDER measurements at the Jornada transition site. Since the sampling angles of POLDER measurements are at different azimuthal plane, only the scattered plot is shown here. The stars are the POLDER measurement and the diamonds are the GORT-Hapke model prediction.

nada site. We are not expecting the difference on the BRDFs measured from the AVHRR and POLDER sensors in the Jornada site.

Model Prediction

The canopy structure input parameters for the GORT model are listed in Table 1. The leaf transmittance and reflectance inputs are listed in Table 2. They are all from Asner et al. (2000). Notice that the values of leaf transmittance and reflectance are weighted values of two species: mesquite (80%) and yucca (20%) since they are the two dominant species. The proportion of diffuse skylight is 5–10% in visible and 10% in near-infrared (measured by the USDA UVB Radiation Group).

The input parameters for Hapke's soil model are retrieved from the soil BRDF measurements using a SE590 spectroradiometer by Walter-Shea (personal communication). The details can be found in Privette et al. (2000). The single scattering albedo of soil is shown in Figure 3. The only input parameter, the nadir reflectance of the soil background at the solar zenith angles θ_i , for Walthall model, is calculated based on Hapke's soil BRDF model (see Table 2) since no field measurements are available.

For comparison, Figure 4 shows the BRFs in the solar principal plane, which is the plane defined by the direction of illumination and the normal to the surface modeled by Hapke and Walthall models. The Walthall

model is based on a polynomial fitting, and produces a less pronounced hotspot. The difference between these two models are large only at extreme viewing zenith angles in the forward scattering directions, where Hapke's model produces a much larger value than the prediction by the Walthall model.

Figure 5 shows the modeled areal proportions of the four components in the principal plane for the transitional site as a function of viewing zenith angles at solar zenith angle 30° . The areal proportion of sunlit background, K_g , shows a peak value at the hotspot viewing direction, and decreases when the view angle is away from the hotspot angle. It is also shown that K_g decreases when the viewing angle is away from nadir. When viewing zenith angle is less than 60° , the satellite will see more than 50% of the background. The fraction of sunlit crown, K_c , as a function of viewing direction exhibits a bowl shape, with larger values at the backward scattering direction than forward scattering. More vegetation is viewed at very large viewing zenith angles. In this case, when the viewing zenith angle is greater than 70° in the backward scattering, K_c is greater than 50%. The shaded crown proportion K_s shows a zero value at the hotspot angle and increasing values as the viewing angle moves away from the hotspot. Larger values occur when the viewing zenith angle is very large (75°) in the forward scattering direction. The shaded background K_b shows a zero value at the hotspot direction and relatively large

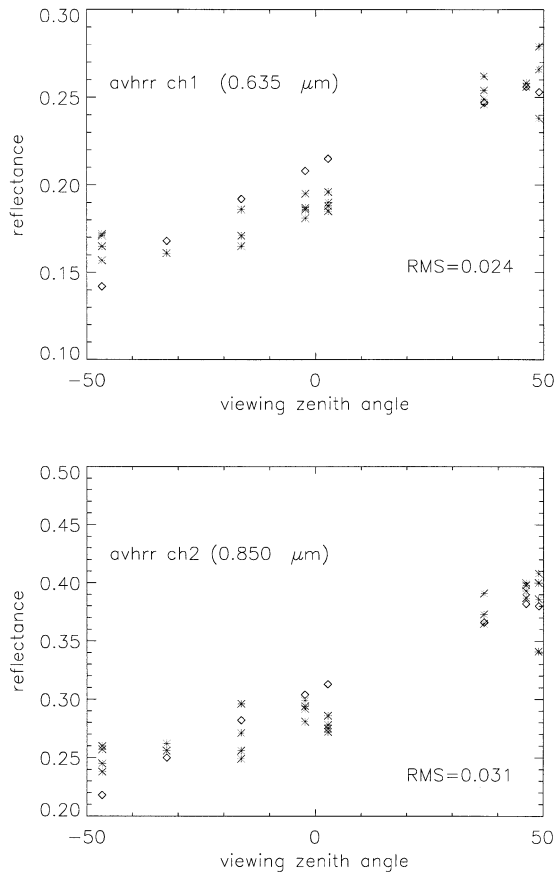


Figure 10. Comparison of the prediction of the surface directional reflectance using a coupled soil-vegetation model with AVHRR measurements at the Jornada transition site. The stars are AVHRR measurements, and the diamonds are the GORT–Walthall model prediction.

values at backward and forward directions. The above patterns of the four components explain the shadowing effect of tree crowns well. At the hotspot, no shadows are observable, so no shaded crown and shaded background can be seen and the sunlit crown and sunlit background are at peak values.

Figure 6 shows the modeled spectral signatures of the four components in AVHRR Channels 1 (visible) and 2 (near-infrared). The spectral signature of sunlit background G shows a larger value at the hotspot. The signature of the sunlit crown C shows a local maximum value at the hotspot direction due to the effect of a leaf level hotspot and larger values when viewing zenith angles are larger due to the larger path length. The signatures of shaded crown T and background Z are modeled as functions of solar zenith angle, but are almost constant. Notice that the background is significantly brighter than the sunlit vegetation in the visible but is very similar in overall brightness in the infrared. This indicates NDVI is use-

less, as expected and observed, to study the semiarid ecosystems in the case of highly bright soils.

Results of Comparison

Figure 7 shows the comparisons of the model predictions using the GORT model with Lambertian background with the AVHRR ch1 ($0.635 \mu\text{m}$) and ch2 ($0.85 \mu\text{m}$) measurements in the quasiprincipal plane. The model predictions underestimate the AVHRR measurements in the backward scattering direction and overestimate them in the forward scattering direction. The root mean square error (RMSE) is 0.037 in AVHRR ch1 (visible) and 0.046 in AVHRR ch2 (near-infrared). The viewing angle dependence of the modeled BRDFs is very similar to the shape of K_g (see Fig. 5), that is, peak values around the hotspot and the nadir, and decreasing BRDF values when the viewing zenith angle away from nadir. This is not surprising since the sunlit background is the dominant factor within the range of 50° viewing zenith angles for the semiarid landscape. This indicates that it is necessary to couple the soil model and the vegetation model in order to correctly model the bidirectional reflectance over a semiarid ecosystem. Using only soil or vegetation BRDF models are not enough for the semiarid ecosystem.

Figure 8 shows the comparison of the modeled bidirectional reflectance in the quasiprincipal plane using the coupled GORT–Hapke model with the AVHRR ch1 and ch2 measurements in the transitional site. The model predictions match well the AVHRR measurements with RMSE 0.023 in ch1 and 0.030 in ch2. A slight overestimation of AVHRR measurements at the forward scattering and slight underestimation of AVHRR measurements around hotspot at the backward scattering are also observable. Figure 9 shows the comparison of the modeled bidirectional reflectance using the coupled GORT–Hapke model with POLDER measurements at four spectral bands in the transitional site. POLDER sampling angles are at varied directions. The comparison results are simple scatter plots. A reasonable agreement between the model prediction and the POLDER measurements is shown. The RMSE are 0.008, 0.009, 0.008, and 0.011 in POLDER $0.443 \mu\text{m}$, $0.67 \mu\text{m}$, $0.765 \mu\text{m}$, and $0.865 \mu\text{m}$. The comparison tends to show slight overestimation by the model for larger values of directional reflectances (closer to hotspot angles) and slight underestimation for smaller values of directional reflectances (in the forward scattering directions). A similar pattern from a 3-D scene model based on radiosity by Qin and Gerstl (2000) was obtained. Qin and Gerstl (2000) use the same Hapke soil model to characterize the soil BRDF. The only difference is their vegetation BRDF model which is quite complicated 3-D scene model. Here we use the very simple GORT model.

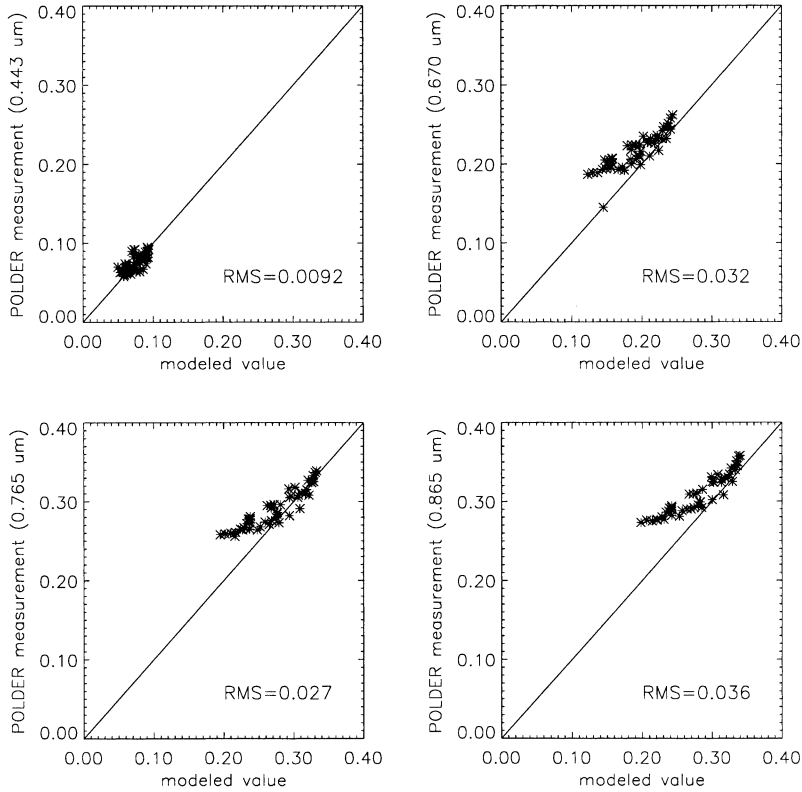


Figure 11. Comparison of the prediction of the surface directional reflectance using a coupled soil-vegetation model with POLDER measurements at the Jornada transition site. The stars are POLDER measurements, and the diamonds are the GORT-Walthall model prediction.

For comparison, the coupled GORT-Walthall model was run to calculate the bidirectional reflectance factor. A reasonably good agreement between the model prediction and the AVHRR is shown in Figure 10. Overestimations of AVHRR measurements around the nadir direction and slightly underestimation of the AVHRR measurements in the forward scattering directions can be seen in Figure 10. The coupled GORT-Walthall model shows better prediction around hotspot directions than the coupled GORT-Hapke model. The RMSEs are 0.024 in ch1 and 0.031 in ch2, almost the same performance as the GORT-Hapke model.

Some deviation of the GORT-Walthall model predictions from the POLDER measurements can be seen in Figure 11. Figure 11 shows the underestimation by the GORT-Walthall model at lower BRDF values. This indicates that the polynomial function of the Walthall et al. (1985) model seems to result in underestimation of POLDER measurements for forward scattering at very large viewing zenith angles since the BRDF values are usually low at those angles compared to other angle samplings (see Fig. 10). One possible reason for the underestimation is the deep drop of the Walthall model at the forward scattering directions (see Fig. 4). The specular effect from the background leads to larger surface reflectance in the forward scattering directions. But the current version of Walthall model with reciprocity cannot adjust such viewing-dependent contrast since the BRDF shape is fixed, with only one parameter which only adjust

the magnitude. Another alternative approach is using the original version of Walthall mode. Without the measurements of the directional reflectance over soil, it is impossible to retrieve the coefficient parameters of the original Walthall model. Notice that only one input parameter is required in Walthall model compared to six input parameters in Hapke's model. Thus it is not surprising that the GORT-Hapke model would be more reliable.

In order to analyze how the background and the canopy components contribute to the total surface bidirectional reflectance, Figure 12 shows the comparisons of predictions based only on Hapke's soil model with the AVHRR measurements. Without the effect of the canopy, the soil model estimates the surface directional reflectance in the backward scattering surprisingly well (with slight overestimation around the hotspot angles), but overestimates the AVHRR measurements significantly in the forward scattering. This is mainly due to the shadowing effect caused by the clumping objects. This indicates that in very sparse plant canopies the shadowing effect of tree crowns affects the bidirectional reflectance in the forward scattering directions more than the backward scattering directions. This effect could prove useful for separating the background and the canopy in the surface parameter retrievals based on directional imagery. Figure 12 also shows a larger overestimation using only the soil BRDF model in the visible than the near infrared. This is primarily due to the fact that the soil and vegetation reflectance are more distinct in the visible

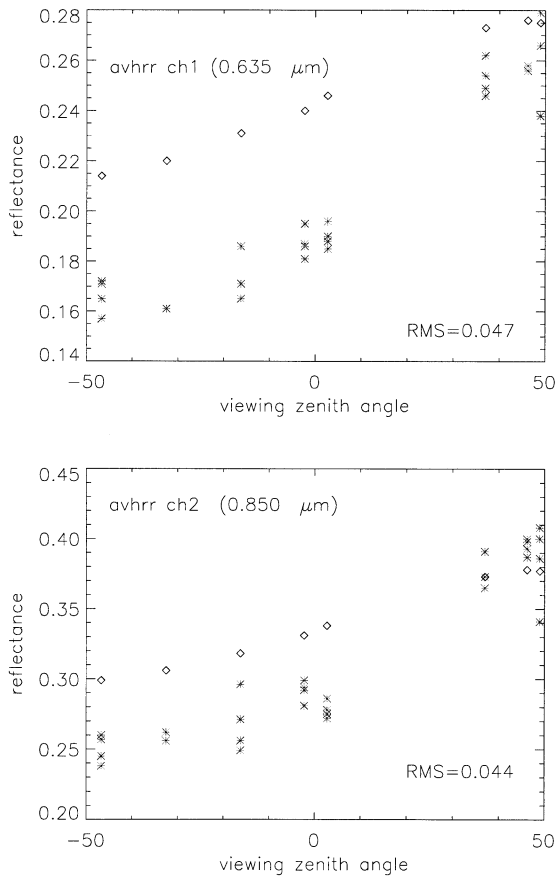


Figure 12. Comparison of the predication of the surface directional reflectance using only a soil model with AVHRR measurements at the Jornada site. The stars are the AVHRR measurements, and the diamonds are the Hapke soil model prediction.

(Fig. 6) than in the near-infrared. So omission of the effect of vegetation is a bigger problem in the visible.

CONCLUSIONS AND DISCUSSION

Vegetation canopy reflectance models assuming a Lambertian background are insufficient to estimate BRDFs in semiarid landscapes with sparse vegetation. Coupling of a soil model with a vegetation model improves the ability to estimate the directional reflectance of a semiarid ecosystem characterized by low fractional cover of vegetation.

The coupled GORT–Hapke model fits the POLDER and AVHRR measurements better than the coupled GORT–Walthall model does. A polynomial fitting in the Walthall model leads to underestimation of the directional reflectances in the forward scattering directions. This contributes to the mismatch between the model prediction and the AVHRR and POLDER measurements.

For very sparse canopies (tree cover less than 30%), validation results show that using only a soil BRDF

model for the very sparse semiarid ecosystem leads to significant overestimation in the forward scattering, due to the shadowing effect of the clumping objects. This effect is not significant in the backward scattering. This information will be helpful in the surface physical parameter retrieval to distinguish the bidirectional effects from the plant canopies and the soil background.

In the Jornada site where the grass and low shrubs are the major canopy cover, composed of discrete plant canopies, a hybrid GORT model that includes the geometric optics (GO) effects and uses radiative transfer (RT) to parametrize the signatures of components, will have potential for retrieving vegetation structure parameters. Future research will attempt the unmixing of the components using the fusion of multiangular (such as from AVHRR and POLDER) and hyperspectral (such as from AVIRIS data) to retrieve the surface canopy structure parameters such as densities of different species, their height and crown width. The approach proposed by Asner et al. (1997) can be used for future study. Estimation of vegetation cover and canopy structure from remote sensing data can be used in regional scale models to study the effects of climate change on water and energy balance, and the carbon cycle.

The authors are in great debt to Jeffrey L. Privette for providing the fitted parameters for soil BRDF and AVHRR data, to Greg P. Asner for providing canopy structure information, and to Marc Leroy and other POLDER group members for providing the POLDER data. The authors thank Wenhan Qin and Curtis E. Woodcock for useful inputs, and the anonymous reviewers for their thorough and helpful comments.

REFERENCES

- Abuelgasim, A. A., Irons, J. R., Privette, J. L., Kovalick, W., Dabney, P., and Russell, C. A. (1999), Inversion of a physically based BRDF model using neural networks and ASAS directional Data. *Int. J. Remote Sens.*, submitted.
- Asner, G. P., Wessman, C. A., and Privette, J. L. (1997), Unmixing the directional reflectance of AVHRR sub-pixel land-cover. *IEEE Trans. Geosci. Remote Sens.* 35(4):868–878.
- Asner, G., Wessman, C. A., Bateson, C. A., and Privette, J. L. (2000), Impact of tissue, canopy, and landscape factors on the hyperspectral reflectance variability of arid ecosystems. *Remote Sens. Environ.* 74:69–84.
- Barnsley, M. J., Hobson, P. D., Hyman, A. H., Lucht, W., Muller, J.-P., and Strahler, A. H. (2000), Characterizing the spatial variability of broadband albedo in a semidesert environment for MODIS evaluation. *Remote Sens. Environ.* 74:58–68.
- Hapke, B. (1981), Bidirectional reflectance spectroscopy. *J. Geophys. Res.* 86(B4):P3039–P3054.
- Holben, B. N., Eck, T. F., Slutsker, I., et al. (1998), AERONET—a federated instrument network and data archive for aerosol characterization, *Remote Sens. Environ.* 66:1–16.
- Irons, J. R., Weismiller, R. A., and Peterson, G. W. (1989), Soil

- reflectance. In *Theory and Applications of Optical Remote Sensing* (G. Asrar, Ed.), Wiley, New York.
- Jacquemoud S., Baret, F., and Hanocq, J. F. (1992). Modeling spectral and bidirectional soil reflectance. *Remote Sens. Environ.* 41:123–132.
- Kimes, D. S., Norman, J. M., and Walthall, C. L. (1985), Modeling the radiant transfers of sparse vegetation canopies. *IEEE Trans. Geosci. Remote Sens.* GE-23(5):695–704.
- Li, X., and Strahler, A. H. (1986), Geometric-optical bidirectional reflectance modeling of a coniferous forest canopy. *IEEE Trans. Geosci. Remote Sens.* GE-24:281–293.
- Li, X., and Strahler, A. H. (1992), Geometric-optical bidirectional reflectance modeling of discrete crown vegetation canopy: effect of crown shape and mutual shadowing. *IEEE Trans. Geosci. Remote Sens.* GE-30(2):276–292.
- Li, X., Strahler, A. H., and Woodcock, C. E. (1995), A hybrid geometric optical-radiative transfer approach for modeling albedo and directional reflectance of discontinuous canopies. *IEEE Trans. Geosci. Remote Sens.* 33:466–480.
- Ni, W., Li, X., Woodcock, C. E., Caetano, M. R., and Strahler, A. (1999), An analytical hybrid GORT bidirectional reflectance model for discontinuous plant canopies. *IEEE Trans. Geosci. Remote Sens.* 37(2):987–999.
- Nicodemus, F. E., Richmond, J. C., Hsia, J. J., Ginsberg, E. J., and Limperis, T. (1977), *Geometrical Considerations and Nomenclature for Reflectance*, Natural Bureau of Standards Monograph 160, Institute for Basic Standards, Washington, DC.
- Nilson, T., and Kuusk, A. (1989), A reflectance model for the homogeneous plant canopy and its inversion. *Remote Sens. Environ.* 27:157–167.
- O'Brien, D. M., Mitchell, R. M., Edwards, M., and Elsum, C. C. (1998), Estimation of BRDF from AVHRR short-wave channels: test over semiarid Australian sites. *Remote Sens. Environ.* 66:71–86.
- Pelgrum, H., Schumugge, T., Rango, A., Ritchie, J., and Kustas, B. (1998). Spatial variability of thermal and near infrared imagery in JORNEX. In *IEEE International Geoscience and Remote Sensing symposium Proceedings*, 6–10 July 1998, Seattle, USA, pp. 589–591.
- Privette, J. L., Abuhassan, N., Holben, B., and Asner, G. P. (2000), Field measurement, scaling and satellite validation of surface bidirectional reflectance. *Remote Sens. Environ.*, (submitted).
- Qin, W., and Gerstl, S. A. (2000), 3-D scene modeling of Jornada semi-desert vegetation cover and its radiation regime. *Remote Sens. Environ.* 74:145–162.
- Schlesinger, W. H., Reynolds, J. R., Cunningham, G. L., et al. (1990), Biological feedbacks in global desertification. *Science* 247:1043–1048.
- Sellers, P. J., Meeson, B. W., Hall, F. G., et al. (1995), Remote sensing of the land surface for studies of global change: models—algorithms—experiments. *Remote Sens. Environ.* 51:3–26.
- Staylor, W. F., and Suttles, J. T. (1986), Reflection and emission model for deserts derived from Nimbus 7 ERB scanner measurements. *J. Clim. Appl. Meteorol.* 25:196–202.
- Strahler, A. H. (1997), Vegetation canopy reflectance modeling—recent developments and remote sensing perspectives. *Remote Sens. Rev.* 15:179–194.
- Strahler, A. H., and Jupp, D. L. B. (1990), Modeling bidirectional reflectance of forests and woodlands using Boolean models and geometric optics. *Remote Sens. Environ.* 34: 153–160.
- Walthall, C. L., Norman, J. M., Welles, J. M., Campbell, G., and Blad, B. L. (1985). Simple equation to approximate the bidirectional reflectance from vegetative canopies and bare soil surfaces. *Appl. Opt.* 24:383–387.
- Wanner, W., Li, X., and Strahler, A. H. (1995), On the derivation of kernels for kernel-driven models of bidirectional reflectance. *J. Geophys. Res.* 100:21,077–21,089.